



PANTOGRAPH ARC EROSION SIMULATION OF HIGH-SPEED RAIL WITH ANSYS SOFTWARE

Kaveen Ranasinghe, and Hassan NOURI
Energy and Power Institute, Bristol, UK

Abstract— ANSYS finite element analysis software is used with the aim of gaining a deeper understanding of arc erosion in pantograph systems. Potential solutions are identified for arc erosion reduction and to overcome the challenges faced by the railway industry in terms of increased operational costs, traction power losses and system malfunctioning. The study evaluates the performance of various contact materials, including pure graphite, pure copper, and two graphite-copper composites (C-Cu60 and C-Cu32), under simulated arc conditions. The results demonstrate that the material composition and its inherent thermal properties, such as thermal conductivity and boiling/sublimation point, are the primary factors influencing arc erosion. Among the materials tested, the graphite-copper composite with a higher graphite content (C-Cu32) exhibits the lowest overall erosion rates, due to the exceptional thermal tolerance and high sublimation point of graphite. In contrast, pure copper is more susceptible to rapid vaporization due to its lower boiling point, while the C-Cu60 composite, with a higher copper content, performs better than pure copper but is outpaced by the C-Cu32 variant. These findings correlate well with those reported by Mersen Transport Company. Analysis of temperature profiles, erosion rates, and crater formations provide valuable insights into the development of pantograph material selection.

Keywords— Contact Material, Catenary and Pantograph Arcing, Erosion Simulation with ANSYS FE

I. INTRODUCTION

Electrification of the railway industry has been a prominent move towards the public transportation industry of highly efficient, low emission and quiet operation compared to other means like diesel engines. Electrification was implemented around the late 1800s and has utilized overhead wires to transmit power to the locomotives from steel rods [1]. In pantograph-catenary system power transmission, catenary is the system of overhead wires that supply electricity to the locomotive and a pantograph is a system mounted on top of the locomotive consisting of articulated arms that extend and retract to engage/disengage with the catenary as shown in Fig. 1.

The contact strip mounted to the pantograph collects the current conducted through the catenary wire [2]. Although pantographs are widely used, there are complicated issues regarding the accelerated degradation from electric arcing events. The intense heat concentrations can rapidly erode the strip causing issues, such as increasing the cost of operations, traction power loss, signaling systems malfunctions, causing major delays and damage to the transport industry.

For the past five decades, theoretically the arc's effect on contacts has been discussed by scientists through the creation of different mathematical models (mainly in the form of isotherms) via the use of analytical methods and numerical methods [5-9]. For example, in recent years, ANSYS was used in electrical contacts by Borkowski et al [10] to simulate thermal conductance, melting and evaporation caused by arcing, Nouri et al [11] to study arc heat distribution on the contact surface, and the Magneto-Hydrodynamics (MHD) approach by Wang et al [12] for the study of contact erosion including both vaporization and sputter erosion. It is worth noting that many of these studies involve simplifying assumptions or focusing on specific aspects of arc behavior, including stable arcing conditions.

As the assessment of pantograph contact erosion in real life or in the laboratory is time consuming, and costly, the main objective of our work is initially (this paper is part 1) to demonstrate how through ANSYS software one can mimic the displacement of pantograph contact material (erosion process) that is the result of crater and pip formation, which as yet has not been investigated through available FINITE ELEMENT packages.

In this work, the simulation data, such as arc temperature, contact area, arc duration, working voltage and current will be taken from an earlier published paper [13]. Also, some assumptions with reference to the boundary conditions, power loss due to the arc column radiation will be made to solely demonstrate the erosion process and the degree of damage on the contact strip for the very short duration of pantograph arcing. Furthermore, under the above simulation conditions, various contact strip materials with different percentages of graphite-copper composite will be tested to establish a foundation for future optimal material composition selection, facilitate the maintenance method, reduce operational costs and enhance pantograph performance efficiency. Our next paper (part 2) will report on the construction of a laboratory test rig based on the above ANSYS model. A comparison of the results serves not only as further concrete validation of

simulated results but also aids the explanation of some findings observed in simulation and experimental work which would otherwise remain unclear.

The organization of the paper is as follows: Section I introduces the background to the research in this area and the work of this paper. Section II discusses the formation of the arc in pantograph systems. Section III describes the arc erosion, section IV presents the selection of data from the reference paper [13] as well as how the arc power is calculated for simulation purposes and section 5 discusses a sample of the simulation results, which confirms findings of Mersen [3] where to date the optimum sintered composite material is C-Cu32.

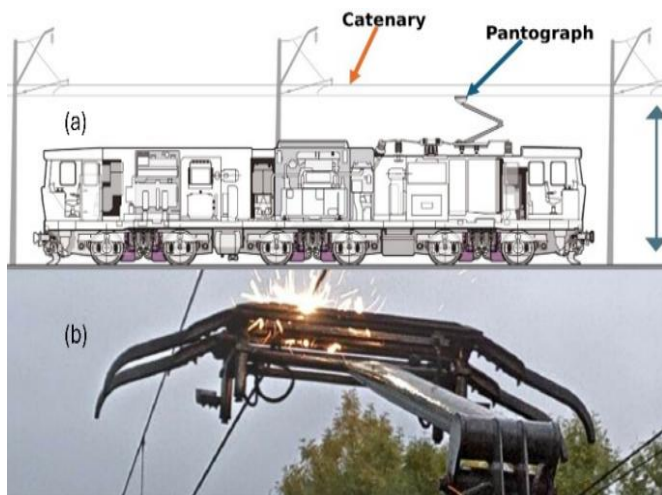


Fig. 1. System view [3] (a) and Pantograph arcing [4] (b)

II. ARC FORMATION AND ISSUES IN PANTOGRAPH-OVERHEAD WIRE SYSTEMS

An electrical arc is a discharge that occurs when electrons collide with gaseous atoms or molecules, ionizing them creating a conductive plasma bridge between two conductors, resulting in a highly concentrated transient heat flow with a bright flash. In pantograph systems, arcs can form when the sliding contact momentarily separates from the overhead wire, allowing current to bridge the gap [14].

When the voltage between the wire and the pantograph reaches a certain level known as cathode fall voltage or approximates to arc voltage, this leads to arcing as shown in Fig. 1(b). In highspeed current collection systems an arc can result from, for example, misalignment, debris, weather conditions, switching wires and vibration which contributes towards creating a gap. In the stationary pantographs connection/disconnection process two types of arcs exist:

- Breaking type pantograph arc - The arc forms at the instance where a pantograph detaches from the overhead wire. With the increase in disconnection distance, the actual electric field within the slide and wire progressively declines. In instances where the electric

field becomes weaker than the dielectric strength of the air, the arc extinguishes [15].

- Closing type pantograph arc - The arc exists an instant after the pantograph slide and contact wire separate, and just before they re-join together and extinguish at perfect contact [15].

III. ARC EROSION

During arcing, the contact surface receives high temperature heat and as a result the material is subject to rapid phase changes, often in high power arcing scenarios they undergo evaporation or sublimation [16]. This study focuses on thermal erosion caused by the intense heating from the electrical arc acting as a localized heat source. Within the arcing process the anode is subjected to electron bombardment and the cathode with positive ions. The material's surface temperature reaches a boiling point, contact metal disintegrates and craters will form through evaporation.

In this paper the crater formation will be shown with the use of ANSYS FEA (Finite Element Analysis). For a simulation approach involving different materials and composites, the most efficient method to measure erosion rates is in terms of volume loss over time. This approach provides a more direct understanding of how quickly the material degrades, regardless of density variations.

Arc erosion is a multi-phase process. As the thermal energy reaches the material, it melts and vaporizes the material at the contact point, creating molten deposits. When the temperature exceeds the boiling point of the material, this vapor undergoes ionization under the intense heat, forming a plasma that conducts a steady flow of arc current.

Under these extreme conditions, among all the known materials, graphite is more likely to undergo sublimation, directly transitioning from a solid to a gaseous state, bypassing the liquid phase. In general, the combination of arc erosion and mechanical wear develops a complex dynamic degradation process.

Although the arcing events are transient and short lived, the material loss, surface irregularities can accelerate fatigue damage and crack propagation. Predicting the overall damage in real world setup is challenging due to the chaotic nature of arc formation.

IV. ARC DATA AND GOVERNING EQUATIONS

With reference to the study by Gao et al [13], the catenary system is a single-phase alternating voltage of 27.5kV which provides power to the pantograph strip resting on the train and this voltage is passed through the locomotive step-down transformer then rectified, regulated, and inverted by train traction converters. Their study on pantograph arcing at a train speed of 200 km/h observed a gradual increase in arc voltage over time, revealing a stable arc voltage fluctuation between 277V and 400V, while the arc current remains consistently at 75A as shown in Fig. 2. Also, the lasting arc time is reportedly

between 38.4 to 1131.6 ms and the arc radius is in the region of 5 mm.

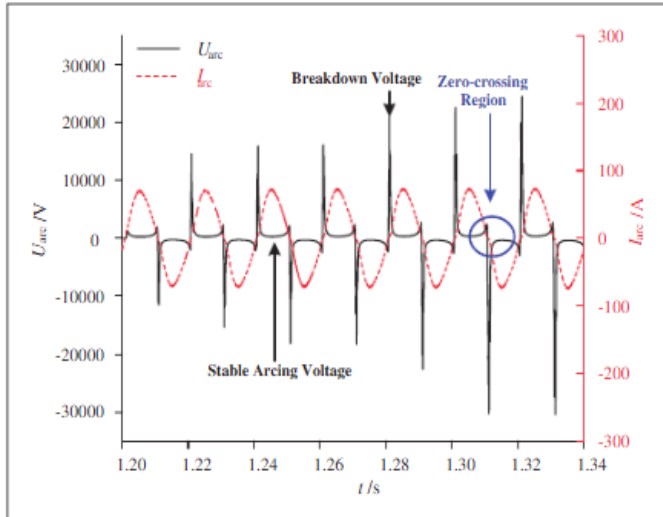


Fig. 2. Depicts Gao et al [13] measured arc voltage and current at a train speed of 200 Km/h.

To investigate the arc erosion effects in our study, and allow for a balanced analysis of transient and stable state arcing conditions, the following parameters that are taken from Gao et al [13], will be selected for calculation and ANSYS simulation purposes:

- Arc voltage: $V_{arc} = 400 \text{ V}$
- Arc current: $I_{arc} = 75 \text{ A}$
- Arc surface area: $A_{arc} = \pi R^2$
- Arc radius: $R_{arc} = 5 \text{ mm}$
- Arc duration: $t_{arc} = 500 \text{ ms}$

It is worth mentioning that while our reference paper, known as Gao et al [13] focuses on the dynamics of moving arcs, our work adopts a focused approach by analyzing a snapshot in time of the transient arc behavior in which a simplified stationary arcing arrangement is simulated with ANSYS and the arc is a forced heat source.

Calculation of the arc intensity (C_b), energy (E_{arc}) and power (P_{arc}) will be performed with the above selected parameters and the following governing Eq. (1) - (3):

$$P_{arc} = V_{arc} \times I_{arc} \quad (1)$$

$$E_{arc} = P_{arc} \times t_{arc} \quad (2)$$

$$C_b = \frac{P_{arc}}{A_{arc}} \quad (3)$$

The calculated values will be recorded by ANSYS ‘Moving heat source’ extension, and by incorporating the eq. (4), a Gaussian heat Q will be applied on a specified surface where R_{arc} is the radius of the contact arc, C_b the source power intensity, x_0 , y_0 and z_0 represent instantaneous positions of the center of the heat flux, whereas x , y and z represent the positions of path coordinates.

$$Q = C_b \cdot \exp\left(-\frac{(x - x_0)^2 + (y - y_0)^2 + (z - z_0)^2}{R_a^2}\right) \quad (4)$$

Table -1 Experiment Result

	Original Lena Image (PSNR)	Watermarked Lena Image (PSNR)
BJUT Watermark Image	33.1224	41.9946
Bobol Watermark Image	33.1224	47.5911
DDNT Watermark Image	33.1224	45.8103

Table 1 show the peak signal to noise ratio of performance of our proposed method of watermarked image and original image with various watermark image, where our watermarked images peak signal to noise ratio has a better performance than others.

V. PANTOGRAPH ARC EROSION MODEL IN ANSYS

To simplify the model and reduce computational time, this study focuses on the direct interaction between the arc and the pantograph contact surface, omitting the overhead catenary wire.

An axisymmetric arrangement is used, enabling the mirroring of symmetrical thermal effects. This mirroring provides a comprehensive analysis of the thermal response and the formation of erosion craters. To represent the arc, a stationary heat source with a fixed diameter is used as shown in Fig. 3. While the length/height of the heat source may be adjusted to reflect the changing dimensions of the damaged area across subsequent tests, the overall intensity and effectiveness of the source remain consistent.

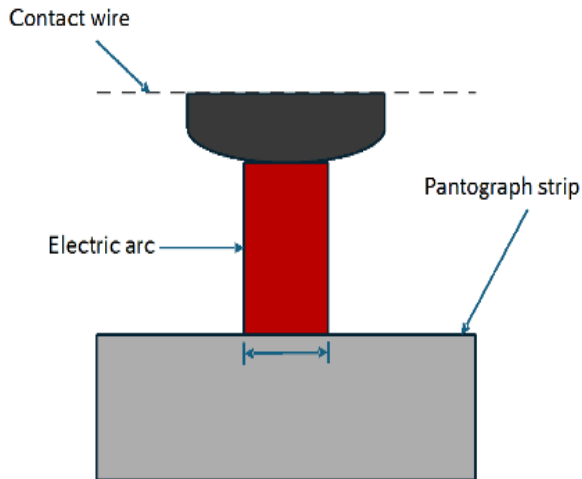


Fig. 3. Simplified geometrical model of pantograph-catenary arc.

a. MODEL SETUP

- (i) The arc is treated as a stationary and time invariant Gaussian heat source of fixed diameter.
- (ii) Model symmetry is used for a reduction in computational stress.
- (iii) Depositions, porosities, and other micro-structural effects are not explicitly modelled.
- (iv) Heat losses due to radiation are assumed negligible compared to conduction/convection and transient behavior.
- (v) Only a small strip section is modelled, assuming negligible global pantograph deformation
- (vi) The catenary wire geometry is excluded, focusing solely on the pantograph strip's response.

b. BOUNDARY CONDITIONS

The boundary conditions utilized on the models are designed to accurately capture the heat transfer mechanism during the erosion process. A convective boundary condition is applied to the top face of the model to experience the exposure to open environment in which the arc contact takes place, the convective heat transfer coefficient is treated as temperature dependent allowing for variation with temperature gradient. Given the model represents only a selectively sampled portion from the pantograph strip, the adjacent face of the portion remains within the material, shielded from the environment and defines conduction behaviour. Radiation heat losses are typically negligible compared to the magnitude of convection and conduction effects during arcing events. Further studies may incorporate radiation modelling for an increased understanding.

c. MESH SELECTION

Meshing plays a crucial role in resolving high temperature gradients and capturing the transient complexities of the arc phenomenon. A separate, iterative mesh convergence study

was conducted to determine the optimal mesh density, ensuring a balance between computational cost and accuracy. To ensure consistent erosion analysis across all samples, the area directly susceptible to arc erosion maintains a uniformly fine mesh with an element size of 0.1mm. This eliminates potential variability in calculated volumes, mass loss, and other erosion-related metrics that could arise from different meshing strategies. For the rest of the model, a coarser mesh is sufficient, as thermal fluctuations are less pronounced.

The mesh consists of structured hexahedral elements, for superior accuracy and convergence compared to tetrahedral elements. The structured hex mesh seamlessly suits the rectangular geometry of the pantograph strip section, minimising potential discretisation errors.

d. MATERIAL SELECTION

Copper is a widely used material in pantograph catenary systems due to its excellent electrical conductivity, thermal conductivity, and corrosion resistance. However, it has low strength and softening temperature making it a poor thermal resistor leading to increased susceptibility to arc erosion. Compared to other material samples for the contact slides, copper contacts are more prone to failure under the demands of high-speed locomotives operations, potentially risking the reliability of the system [2]. The simulation results will demonstrate this vulnerability to highlight the thermal erosion effects.

Pure carbon is a common choice for contacts due to its self-lubricating properties. As the overhead wire slides across the carbon strip, a lubricating layer forms, which significantly benefits the prolonged life of the strip. Additionally, carbon strips generate low electromagnetic noise, high temperature resistance and absence of welding effect when exposed to high powered arcs [2].

To improve the overall erosion performance of contacts, sintered composite material of carbon and copper with 60% Cu and 40% C by mass is reported [2]. This is related to its thermal management capabilities (superior arc erosion resistance) and lubrication ability.

More recently Mersen [3] has developed a wide range of carbon grade materials to meet even the most demanding operating conditions, such as pantograph contact materials (Grade P3210) with 32% copper content. This is related to an increase in its thermal resistance and boiling point.

In our work, graphite (C) and copper (Cu) data are sourced through the "ANSYS Granta Edu Pack" software. For composite structures, the method of linear combination/mixing is used to identify the material properties based on the respective copper and graphite content present as depicted in Table I. This approach follows the methodology used by Wang et al. [17], using the expression shown below:

$$X = k \cdot X_C + (1 - k) \cdot X_{Cu} \quad (5)$$

In eq. (5), x represents the physical parameter of the composite and k is the mass percentage of C in the composite,

X_C represents the physical parameter of C (graphite) and X_{Cu} is the physical parameter of Cu (copper).

Table 1. Parameters of Various Materials.

Material	Content(w)	Density(kgm ⁻³)	Boiling/Sublimation point(°C)	Thermal conductivity (Wm ⁻¹ °C ⁻¹)
Graphite (C)	100%	2260	4200	240
Copper (Cu)	100%	8954	2562	398
Graphite-Copper (C-Cu60)	40% C, 60% Cu	6276	3217	335
Graphite-Copper (C-Cu32)	68% C, 32% Cu	4402	3676	291

It is worth noting that when calculating physical parameters in sintered composite structure, different materials possess different physical parameters. For example, in the case of C-Cu60 or C-Cu32, when the effective temperature is below 2562°C, the boiling temperature of copper, both metals in the composite structure remain solid without vaporisation (melting is not assessed). When the temperature is above 2562°C and below 4200°C, the copper in the composite structure vaporises, turning into gas.

e. ANSYS FLOW CHART FOR EROSION PROCESS

ANSYS transient thermal provides an ideal platform for the study of arc erosion phenomenon. Irrespective of the arc being modelled as a stationary Gaussian heat source, the resulting heat transfer characteristics and material response are fundamentally transient processes. ANSYS finite element analysis transient thermal allows to capture this time evolving of temperature fields through convection, conduction, and radiation effects essential for the accurate thermal modelling of arc erosion. Furthermore, it allows for advanced meshing techniques to simplify the solving process and to reduce computational stress. The ‘Element KILL (EKILL)’ option can be altered using ANSYS Parametric Design Language (APDL) where the software allows for a wide range of customisation for the necessary application, whereas the element deactivation occurs when a certain limit is reached. This effectively simulates the volume change (Δv) due to erosion. Fig. 4, serves as a graphical representation outlining the procedural steps undertaken in each individual test, where the ‘repeat test’ pathway, subjects the model to be analysed again for erosion. The software chooses and executes the parameters specified on the simulations and applies heat for the predesignated point. A conditional statement determines whether the model has reached a certain threshold temperature, typically it is the predefined boiling point of the specific material triggering the erosion process.

The ANSYS EKILL command utilized is a powerful tool for simulation of material failure with transient analysis. EKILL does not remove but instead deactivates the element where it remains in the model but has no impact with near-zero conductivity value to the overall matrix [18]-[20]. The programme checks for the elements and nodes which exceed the designated threshold of boiling point for each material, and it then deactivates the elements which are equal to or more than this certain value. If there are remaining elements with the above-mentioned threshold value it rechecks and loops the deactivation process until it satisfies this condition. After this process is completed, the model is extracted using an ANSYS APDL command which will allow use of the same used model for the next test and so on; effectively simulating the erosion cycles through tests after a pre-determined period of cool down to room temperature.

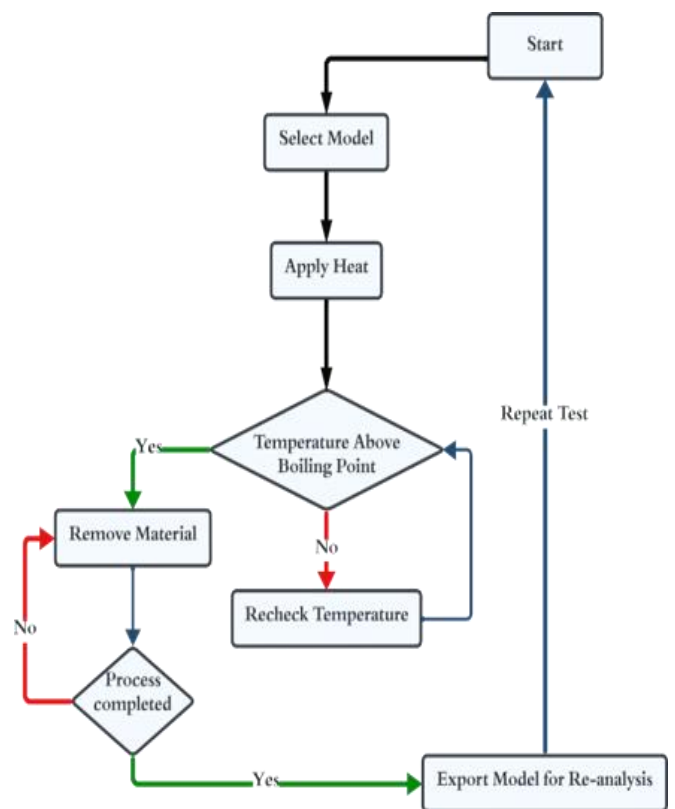


Fig. 4. Graphical representation outlining the procedural steps undertaken in each individual test

VI. RESULTS AND DISCUSSION

For the erosion study, four series of tests (T1, T2, T3 and T4) were conducted, with each test having a duration of 500 ms. In each test four materials, namely, C, Cu, C-cu32 and C-Cu60 are used and the erosion measurements in terms of mass, volume, and temperature are taken every 25 ms. The key factors determining the arc erosion rate of a material can simply be related to its thermal properties, specifically the

boiling point and thermal conductivity. While convection contributes to cooling the exposed surface, its effect remains consistent across all materials in these tests. Due to this consistency, the variation in convection is not a primary factor influencing the observed differences in erosion behaviour between the materials.

To investigate the arc erosion damage propagation from individual arc instances, each simulation test is conducted after the pantograph model is allowed to cool to ambient temperatures before the start of next test T2 (the same condition for T3 and T4).

Fig. 5, shows the average mass erosion of different samples in each test where the composite with the highest copper content (highest density) experiences the more significant mass loss. Also, the sample with greater density, such as copper (8954 kgm⁻³), experiences a greater mass erosion compared to less dense materials such as graphite (2260 kgm⁻³).

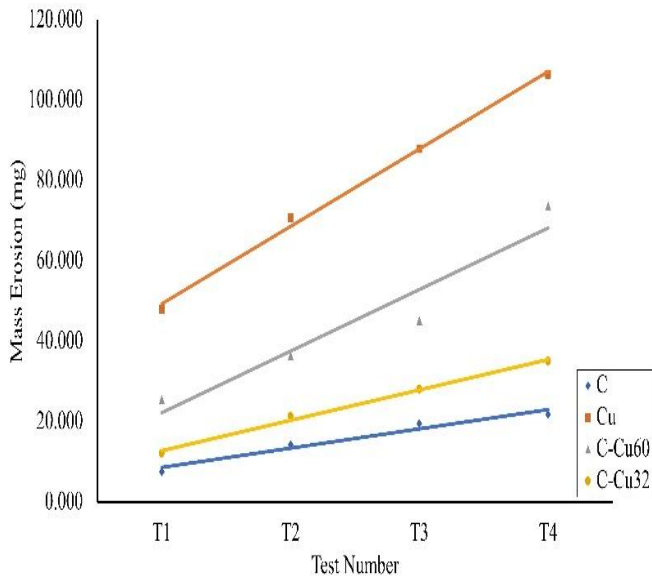


Fig. 5. Variation of mass erosion against each test.

To investigate the impact of thermal conductivity on the materials, maximum temperature profiles for each pure and composite material during a single test with a 500 ms duration is plotted in Fig. 6.

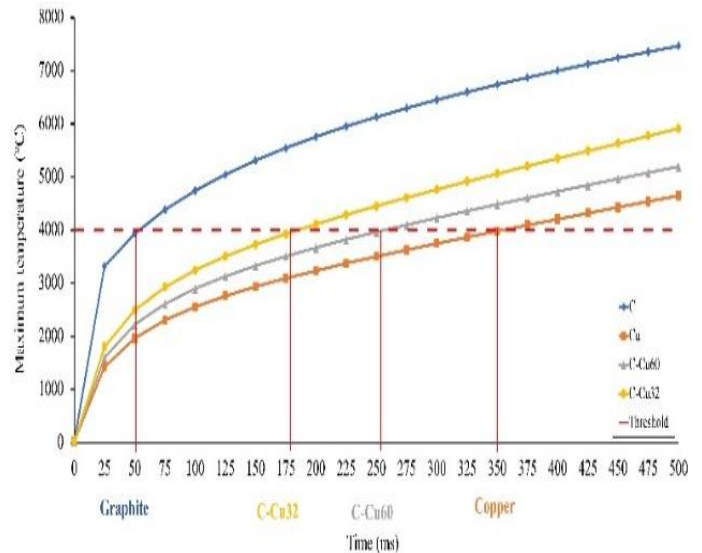


Fig. 6. Maximum temperature variation with time - Erosion disabled.

Analysis of Fig. 6 suggests that these profiles correlate with the corresponding thermal conductivity properties shown in Table 1. A horizontal dashed line at 4000°C (representing the highest boiling temperature) is included as a reference to identify the order in which materials reach this threshold temperature. The time-axis projections of the intersection points support this observation: graphite, with its lower thermal conductivity, reaches the reference line first, while copper takes the longest time. The C-Cu32 composite, having a higher graphite content, reaches the threshold after pure graphite. Conversely, the C-Cu60 composite, with its higher copper content, achieves this point later than C-Cu32. These results clearly demonstrate the influence of thermal conductivity on the materials.

For erosion taking place at maximum temperatures as shown in Fig. 7, the graphite sample has a sharp increase in temperature from the ambient conditions, reaches maximum, which is above the boiling point of graphite. This indicates that the intense, localized heating from the arc causes the graphite surface to reach its boiling point rapidly, triggering the erosion process. And just after the peak, the drop in temperature represents material loss due to vaporization at the arc contact surface. This is a common phenomenon to all material erosion behavior. The comparatively smoother curve for graphite can be related to the fact that it is a rather poor thermal conductor with a conductance of 240 W/mC°. This limits the heat dissipation from the contact region resulting in a more localised and sustained thermal zone.

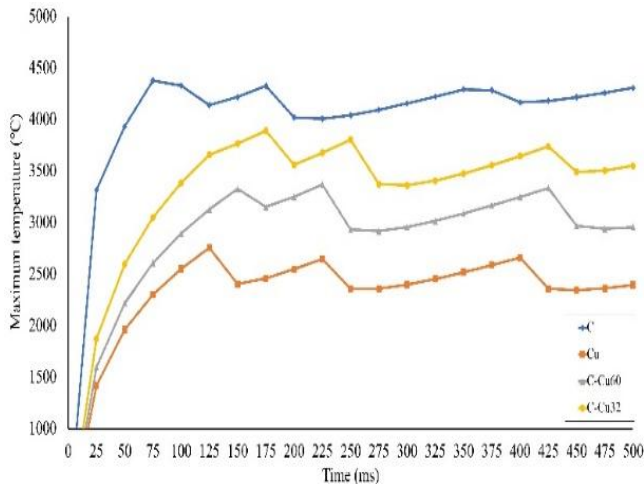


Fig. 7. Maximum temperature variation with time - Erosion enabled.

Considering variation in the density of materials, for the same volume of material loss, a different erosion mass will exist and this in turn could lead to misinterpretations of simulation results. Therefore, by analysing the volume erosion, the comparison between different materials becomes more direct as it reflects actual loss of material from the contact surface. The volume erosion data plotted in Fig. 8, from the four tests (T1 to T4) provides a clear understanding of the performance of the different types of materials. These results also suggest that C-Cu32 exhibits the lowest overall volume erosion among the tested samples.

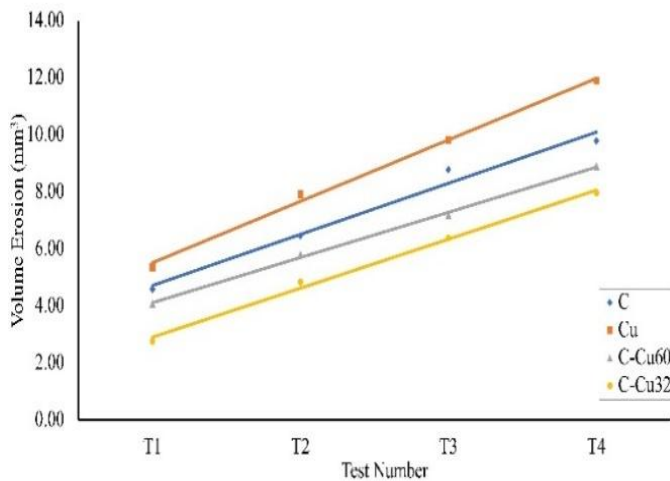


Fig. 8. Volume erosion throughout each test on different materials.

A closer examination of Fig. 8 reveals that in test 1 (T1), the erosion volume for C-Cu32 is 2.76 mm³, which is the lowest compared to the other materials. This trend continues through the subsequent tests (T2 to T4), with the C-Cu32 composite reaching a total erosion volume of 7.9733 mm³ by the end of

test 4 (T4). This is significantly lower than the copper (Cu) sample, which reached 11.9067 mm³ by the end of test 4 (T4). To further emphasise the effectiveness of the C-Cu32 composite over the samples used in this investigation, the erosion rate of various samples is plotted in Fig. 9 in which the lowest erosion rate of 0.0055 mm³/ms is in T1 and gradually increases to 0.0159 mm³/ms in T4.

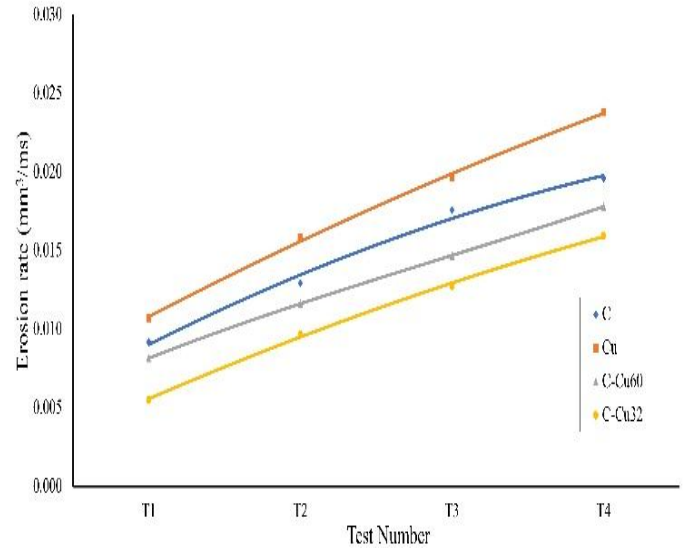


Fig. 9. Erosion rate of different materials in each test.

Erosion behaviour is also dependent on the thermal conductivity of materials. For example, the poor thermal conductivity of graphite is the primary reason for the onset of erosion behaviour, as the material reaches its boiling point faster compared to the other test samples. In contrast, as shown in Fig. 7, copper exhibits a delayed erosion response at 125 ms compared to graphite's sublimation at 75 ms. This is related to the high thermal conductivity of copper (398 W/mC°), which allows the concentration of heat to more efficiently dissipate away from the contact area. This effect is evident from the 3D simulation samples shown in Fig. 10(a)-(b). As a result, the local temperature at the arc-contact interface takes longer to reach the boiling point of copper. Furthermore, despite the thermal conductivity advantages of C-Cu60 the data reveals, it erodes more rapidly than C-Cu32. This is primarily due to its lower boiling point, resulting from a higher copper content. However, graphite's excellent thermal resistance and high sublimation point make it a critical component in reducing arc erosion. Consequently, the composite material with a higher graphite content (C-Cu32) demonstrates superior performance in this study.

The results also indicate that the poor thermal conductivity of graphite leads to a more sustained and concentrated thermal zone at the contact interface (see Fig. 10(a)), causing it to reach its sublimation point faster than the other materials. However, graphite's superior thermal resistance properties

ultimately result in low erosion rates. In contrast, pure copper, with its low boiling point and high thermal conductivity is far more susceptible to rapid vaporisation and material loss. This is related to concentrated heat quickly being dissipated through the copper, leading to the highest erosion rates as observed in simulations at a rate of $0.0238 \text{ mm}^3/\text{ms}$ by test 4 (T4). The C-Cu60 composite, with a higher copper content exhibits intermediate erosion performance between C-Cu32 and pure graphite. Despite the addition of graphite helps to improve the thermal resistance of the composite, the higher copper content still renders it more vulnerable to erosion.

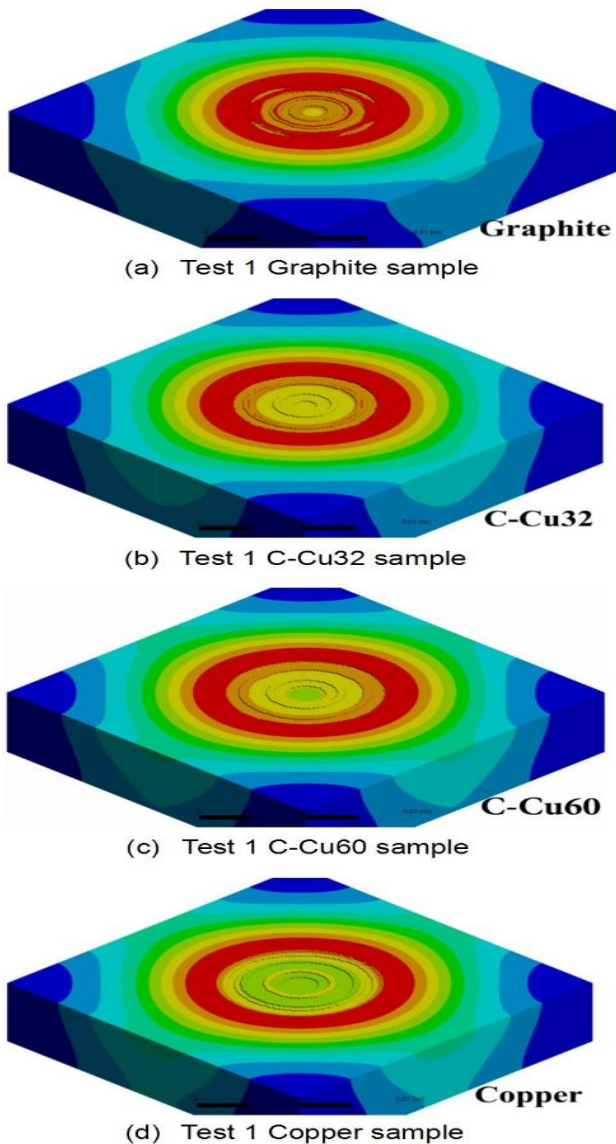


Fig. 10. 3D representation of Test 1 (500 ms duration) for various contact materials.

Referring to Fig. 8 and Fig. 10 (a) to (d), insights into the relationship between a material's thermal conductivity and the

resulting erosion crater characteristics can be recognised. In materials with higher thermal conductivity, such as copper, the efficient dissipation of heat can lead to deeper erosion. This may result in a less concentrated temperature distribution within the erosion pit as the focus of the heat load shifts with the changing geometry of the material. This is reflected in Fig. 10 (d). Graphite, on the other hand, exhibits high-temperature tolerance, while its thermal conductivity is lower than that of copper, it is still capable of conducting heat away from the arc contact area. This, combined with its high-temperature tolerance, contributes to the retention of heat within the centre of the erosion crater. The behaviour of composite materials demonstrates an interplay with arc erosion. The specific composition of the composite, such as the concentration of copper in C-Cu32, influences the depth and distribution of thermal erosion. Notably, C-Cu32 exhibits a shallower erosion crater and a more distributed heat pattern, suggesting a potential for optimised erosion resistance. Fig. 11 to Fig. 14 further demonstrate the latter statement by illustrating the 3D state of the contact obtained via ANSYS simulation every 100 ms (0.1 s) for four contact materials, namely C, C-Cu32, Cu and C-Cu60. Each figure shows the 3D state of the contact for four tests known as T1, T2, T3 and T4. As mentioned earlier, each simulation test is conducted after the pantograph ANSYS model is allowed to cool to ambient temperature at the end of each test and before proceeding to the next test.

VII. CONCLUSION

This study on arc erosion in high-speed railway pantograph systems has provided insights into the complex thermal and material behaviours involved in this critical phenomenon. Through finite element analysis using ANSYS, the investigation has systematically evaluated the performance of various contact materials without considering the speed of the train.

The results clearly demonstrate that the material composition and its thermal properties are the primary factors influencing arc erosion resistance. Among the materials tested, the graphite-copper composite with a higher graphite content (C-Cu32) exhibits the lowest erosion rates across the simulated tests. Graphite, with its exceptional thermal tolerance and high sublimation point, is the primary contributor to the superior performance of the C-Cu32 composite. In contrast, pure copper, despite its high thermal conductivity, is more susceptible to rapid vaporization due to its lower boiling point. The C-Cu60 composite, with a higher copper content, performs better than pure copper but is outpaced by the C-Cu32 variant, highlighting the critical role of optimizing the material blend to achieve superior arc erosion mitigation.

The in-depth analysis of the temperature profiles, erosion rates, and 3-D crater formations have provided a comprehensive insight into the key principles behind arc-induced material degradation.

Finally, extensive FE modelling in conjunction with validation on a laboratory scale model should be performed to define the most relevant parameters and their corresponding values for a

realistic pantograph arc model by considering the effect of train movement and the effects of the arc on the motion of the contacts.

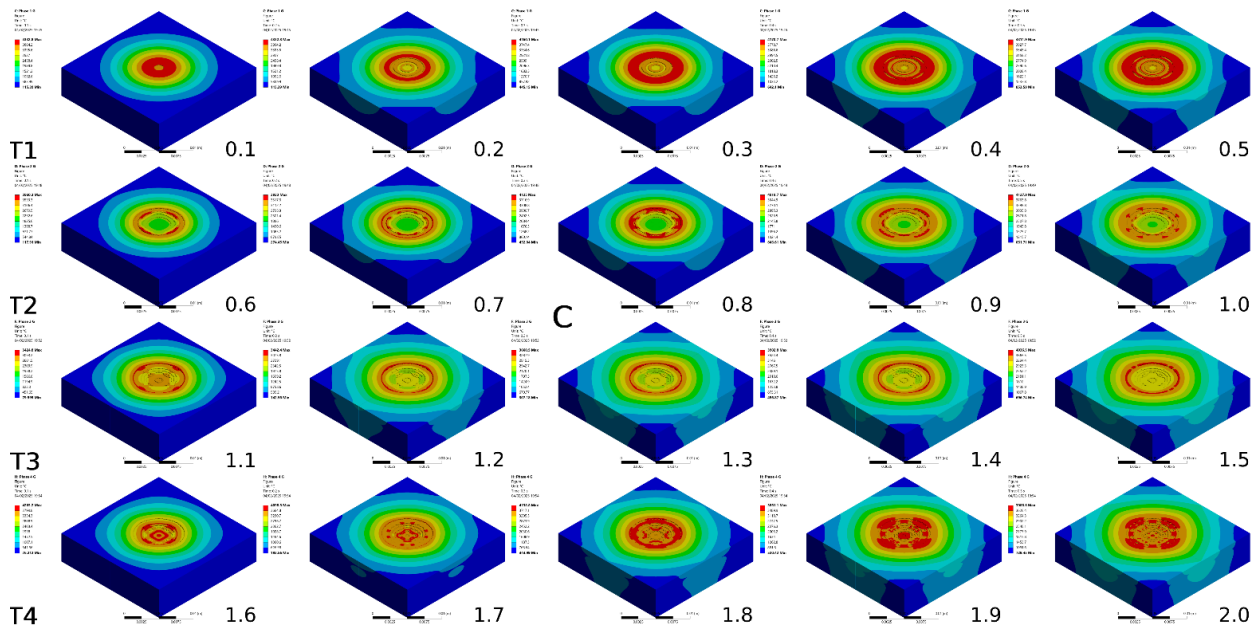


Fig. 11. Shows the 3D state of graphite contact for T1 to T4.

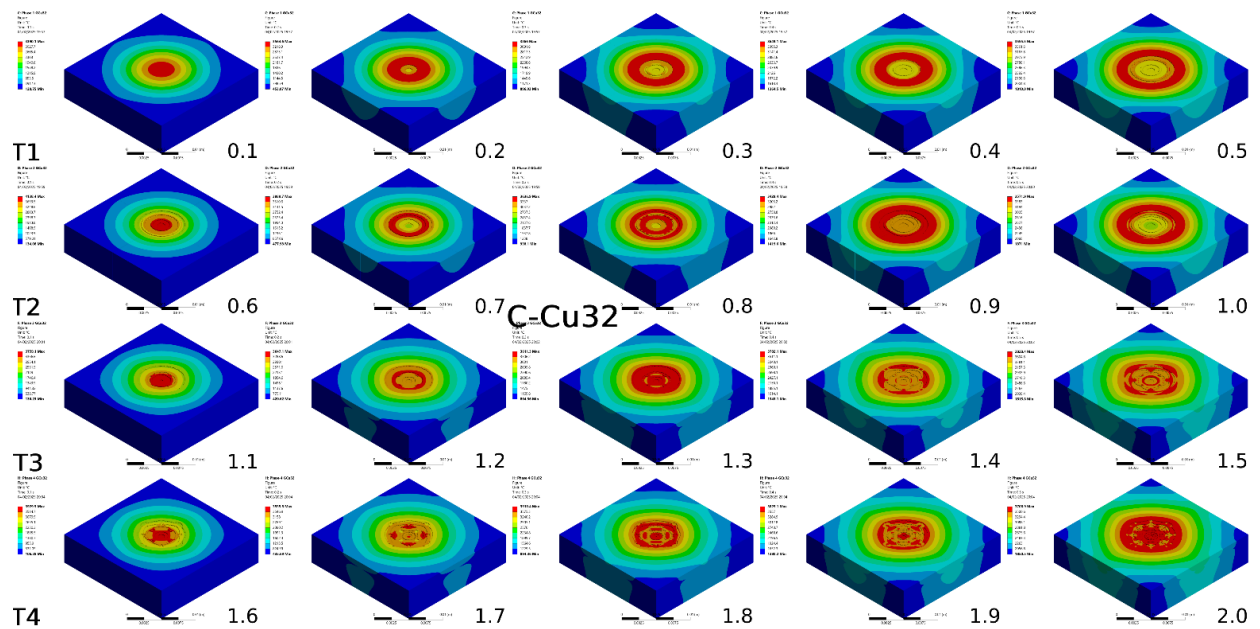


Fig. 12. Represents the 3D state of C-Cu32 contact for T1 to T4.

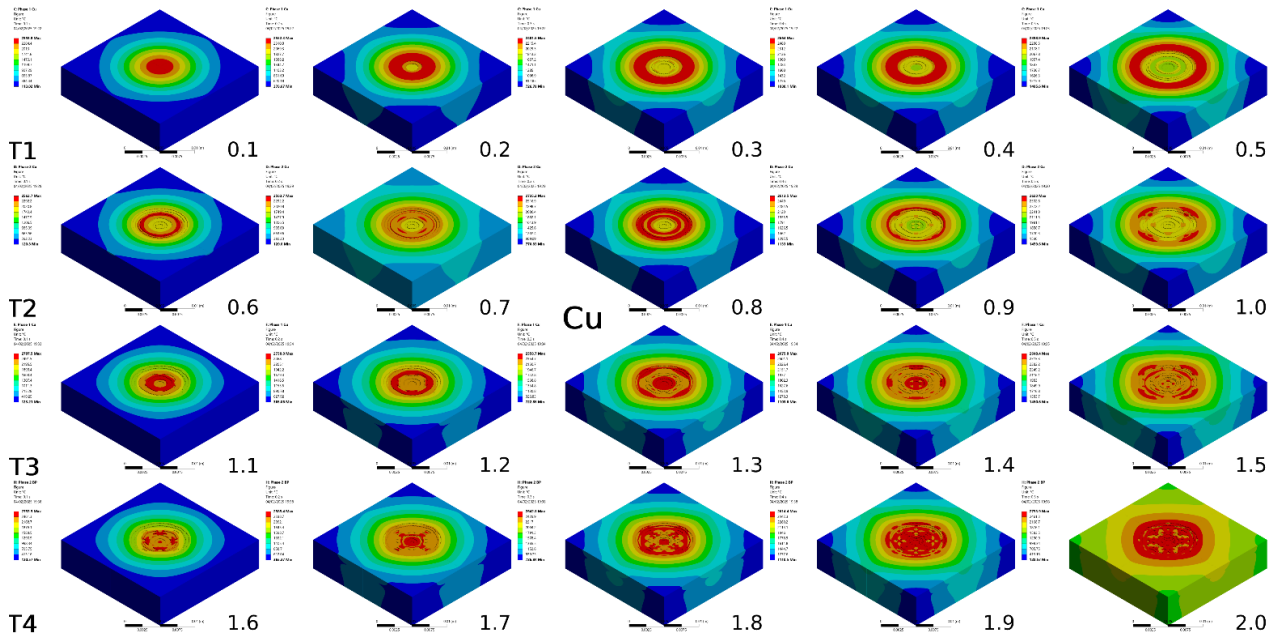


Fig. 13. Depicts the 3D state of copper contact for T1 to T4.

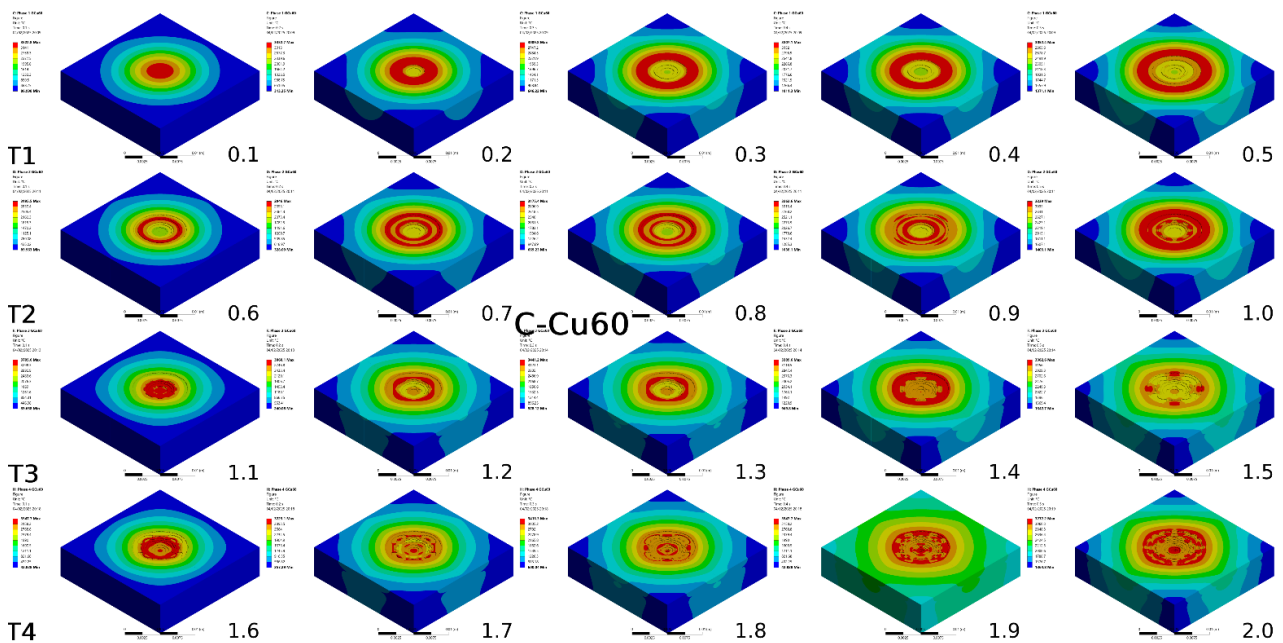


Fig. 14. illustrates the 3D state of C-Cu60 contact for T1 to T4.

VIII. REFERENCE

[1] Hay W. W. (1977). An Introduction to Transportation Engineering, John Wiley & Sons.
 [2] Wu G. et al (2022). Pantograph–catenary electrical contact system of high-speed railways: recent

progress, challenges, and outlooks, Railway Engineering Science, Vol. 30, (pp 437–467).
 [3] MERSEN (2024). Current collection technical guide, available: <https://rb.gy/miehhm>.



- [4] SelectraVISION (2012). System for measuring and counting pantograph arcs, available: <https://www.selectravision.com/pantograph-arcs.php>.
- [5] Lefort A., and Andanson P. (1980). Experimental investigation of the energy exchange process at contacts subjected to an electric arc of intensity less than 3kA, Proc. 10th ICECP, Budapest, (pp129-137).
- [6] Kim E. I and Kharin S. N. et al. (1982). Thermophysical Processes in Electrical Contacts with Short Arc, Proc. 11th ICEC, Berlin, (pp 82-85).
- [7] Nakagawa Y and Yoshioka Y. (1976). Theoretical calculation of the process of contact erosion using one dimensional contact model, Proc. 8th ICECP, Tokyo, (pp 216-220).
- [8] Abadi M. M et al. (2024). A review of simulation and numerical of electric arc furnace (EAF) and its processes, Heliyon, Science Direct, Vol. 10, Issue 11, (pp 1-21).
- [9] Trelles J. P. (2017). Finite Elements Methods for Arc Discharge Simulation, Plasma Processes and Polymer, Vol. 14, Issue 1-2, (pp 1-10).
- [10] Borkowski P. et al. (2015). Contact Erosion Modelling Using ANSYS Computer Software and Experimental Research, Archives of Metallurgy and Materials, Vol. 60, Issue 2, (pp 551- 560).
- [11] Nouri H et al. (1996). Experimental and theoretical study of heat transfer in switches, Proc. of 42nd IEEE Holm Conference on Electrical Contacts, Chicago, (pp 45-49).
- [12] Wang Y et al. (2017). Numerical modeling of contact erosion including both vaporization and sputter erosion, 4th International Conference on Electric Power Equipment-Switching Technology (ICEPE-ST), (pp 1-5).
- [13] Gao G et al. (2017). A Pantograph Arcing Model for Electrified Railways with Different Speeds,” Proceedings of the Institution of Mechanical Engineers, Part F: Journal of Rail and Rapid Transit, Vol. 232, Issue 6, (pp 1-10).
- [14] Yang Z et al. (2020). Influence of the Crosswind on the Pantograph Arcing Dynamics, IEEE Transactions on Plasma Science, Vol. 48, (pp 2822–2830).
- [15] Wang Z et al. (2023). Mathematical model of pantograph arc based on probability distribution of arc parameters, IEEE Transactions on Transportation Electrification, Vol. 9, (pp 2026–2037).
- [16] Wilson W. R. (1955). High-current Arc Erosion of Electric Contact Materials, Transactions of the American Institute of Electrical Engineers Part III, Power Apparatus and Systems, Vol.74, Issue 3, (pp 657-664).
- [17] Wang Y et al. (2023). Numerical simulation and analysis of contact erosion by high-current and low-voltage air arc considering the movement of arc, AIP advances, Vol. 13, Issue 5, (pp 1-13).
- [18] SimuTech Group. (2022). Performing EKILL element death in Ansys Mechanical, Available: <https://simutechgroup.com/performing-ekill-element-death-in-mechanical/>.
- [19] Jaroniek M and Niezgodzinski T. (2015). Element Birth and Death Method Application to Lamellar Crack Analysis, Mechanics and Mechanical Engineering Journal, Vol. 10, No. 1, (pp 63-75).
- [20] Fegade R.S. et al. (2018). Finite Element Analysis of Direct Chill Casting using Concept of Element Birth and Death, International Journal of Recent Technology and Engineering, Vol. 8, Issue. 4, Nov. (pp 1-9).